Electronic Supplementary Material (ESI) for Journal of Materials Chemistry A.

Electronic Supplementary Information (ESI)

En route to a unified model for photo-electrochemical reactor optimisation. I - Photocurrent and H_2 yield predictions

Franky E. Bedoya-Lora,*[a] Anna Hankin[a] and Geoff H. Kelsall[a]

a. Department of Chemical Engineering, Imperial College London, London, SW7 2AZ, UK.

Comparison of two models for efficiency of gas evolution

Vogt model: According to Vogt[1], the efficiency of gas evolution, f_G, depends on the fractional surface coverage (θ), current density and concentration difference between the interface and bulk of the solution.

$$f_G = 1 + K_2 - \left[K_2(2 + K_2) + K_3^2\right]^{0.5}$$

$$K_2 = 1.53\frac{DRT}{d\ P}\theta^{0.5}(1 - \theta^{0.5})\Delta c^2\frac{nF}{j}$$

$$K_3 = k_{Ec'}(1 - \theta)\Delta c\frac{nF}{j}$$

The term K_2 is related to the microconvection and K_3 represents the fraction transferred by macroconvection, being $k_{Ec'}$ the mass transfer coefficient due to macroconvection and estimated by the same author for oxygen (1×10^{-5} m s^{-1}) and hydrogen (2×10^{-5} m s^{-1}) gas evolution. Small variances in the efficiency of gas evolution are achieved when a surface coverage between 0.08 and 0.5 is used. Then, it is safe to assume a surface coverage of 0.1 for low current densities (10 – 100 A m^{-2}). The bubble size was assumed as $d = 50\mu m$. The concentration of hydrogen and oxygen, at the interface of the cathode and anode respectively, was estimated from the figures reported by Shibata.[2, 3] Said experimental points were fitted to a 5 parameter logistic (5-PL) equation in order to obtain the concentration of oxygen or hydrogen as a function of the current density.

$$C_{o_2,H_2} = A + \frac{B - A}{\left(1 + \left(\frac{\log j_{a,c}}{C}\right)^D\right)^E}$$

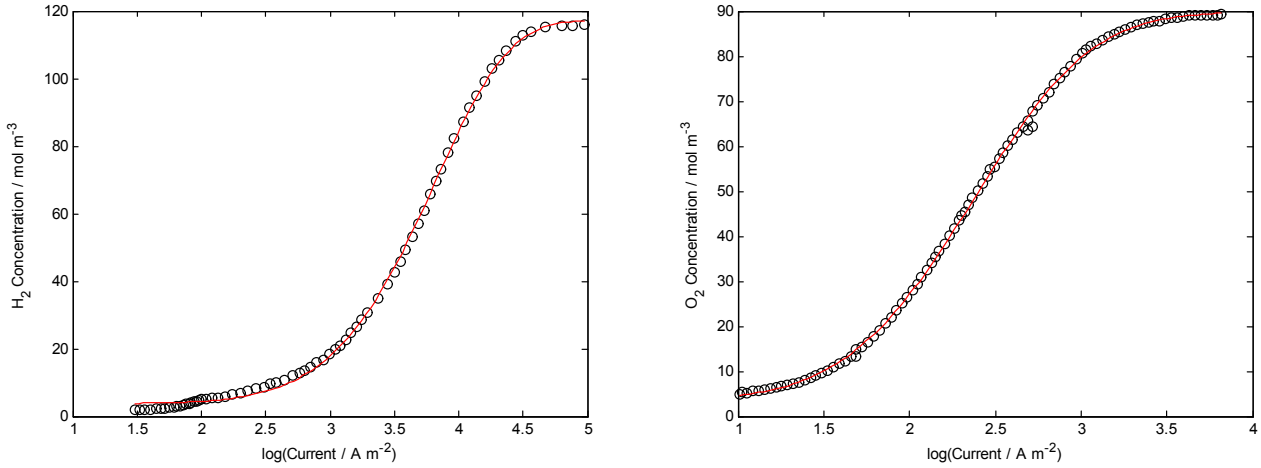

Figure S1. H_2 and O_2 concentration at cathode or anode/electrolyte interface vs current density and fitted data.

Table S1. Fitting coefficients for hydrogen and oxygen concentration as a function of current density.

Constant	H_2	O_2
A	117.98	89.859
B	4.2617	3.7964
C	7.9697	3.7662
D	5.6489	5.0145
E	303.50	7.6856

Janssen model. A simpler relationship for oxygen and hydrogen gas evolution in alkaline conditions is proposed by Janssen et al.[4] It is only a function of current density and ad-hoc parameters found after fitting to experimental data, see Table S5.

$$\frac{f_G}{1 - f_G} = aj^n$$

As it can be seen in Figure S2, both relationships are fairly similar. However, values estimated by Vogt fall into negatives values below current densities of ca. 10 A m^{-2}. This creates a discontinuity in the model which can be avoided if Janssen model is used. Both approaches were successfully used in the model presented to predict the behaviour of photo-electrochemical reactors. However, when using Vogt approach cumbersome restrictions must be applied and longer computing times were required.

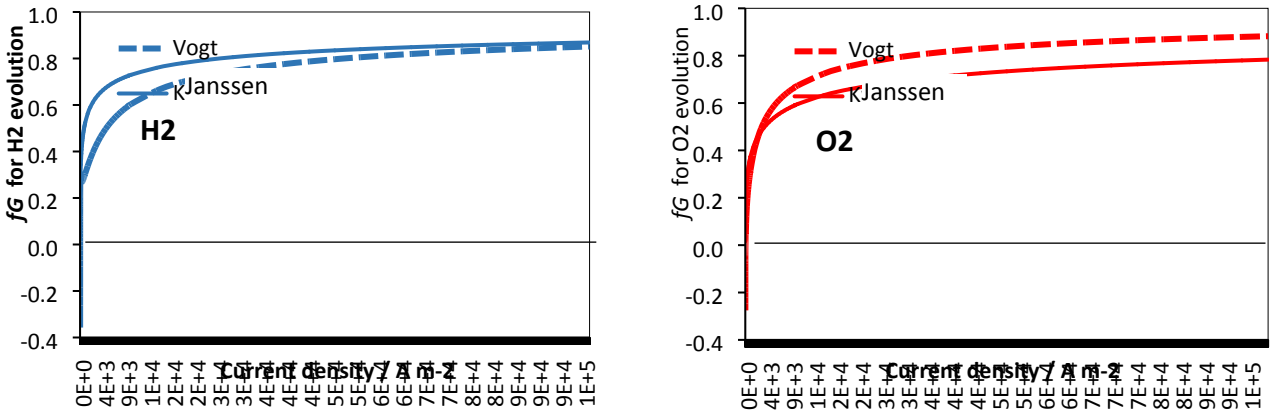

Figure S2. Efficiency of gas evolution for H_2 and O_2 estimated using Vogt (dashed) and Janssen et al. (continuous) relationships

Volumetric mass transfer coefficient estimation for hydrogen and oxygen desorption in water

The volumetric absorption/desorption of gas in the liquid can be expressed in terms of the volumetric coefficient for liquid mass transfer:

$$\frac{dc_i}{dt} = N_{desorption} = K_L a(c_{sat,i} - c_i)$$

$K_L a$ is a function of the hydrodynamic properties of the fluid, diffusivity of the dissolved gas D_i, area of transfer per unit volume a, and characteristic length of the bubble, or in this case Sauter diameter d_B. K_L can be calculated using the Frossling correlation as a function of Re and Sc numbers and the bubble slip velocity, v_B, which can be estimated from Wüest relationship. The area of transfer per unit volume can be estimated using Deckwer correlation in terms of the gas hold up, ε_G, which can be estimated from Joshi and Sharma's correlation.

Table S2. Estimation of volumetric coefficient for liquid mass transfer

Parameter	Symbol	Correlation	Value O_2	Value H_2	Unit	Reference
Sauter diameter of bubble in saturated liquid	d_B		4.50×10^{-4}	4.50×10^{-4}	m	5
Diffusion coefficient of gas in electrolyte	D_i		1.59×10^{-9}	3.00×10^{-9}	$m^2\ s^{-1}$	4
Kinematic viscosity of electrolyte (water at 25°C)	υ		8.90×10^{-7}	8.90×10^{-7}	$m\ s^{-1}$	IAPWS
Bubble slip velocity (relative to liquid)	v_B	$4474\left(\frac{d_B}{2}\right)^{1.357}$	0.0502	0.0502	$m\ s^{-1}$	6, 7
Gas holdup	ε_G	$\frac{v_B}{0.3+2v_B}$	0.125	0.125	1	8, 9
Schmidt number	Sc	$\frac{\upsilon}{D_i}$	559.7	296.7	1	
Reynolds number	Re	$\frac{v_B d_B}{\upsilon}$	25.38	25.38	1	
Mass transfer coefficient	k_L	$\frac{D_i}{d_B}(2+0.6Re^{\frac{1}{2}}Sc^{\frac{1}{3}})$	9.51×10^{-5}	1.48×10^{-4}	$m\ s^{-1}$	10
Area of transfer per unit volume	a	$34.4v_B^{0.25}\varepsilon_G$	2.04	2.04	m^{-1}	8, 11
Volumetric coefficient for liquid mass transfer	$k_L a$		**1.94×10^{-4}**	**3.02×10^{-4}**	**s^{-1}**	
Wüest correlation						
Volumetric coefficient for liquid mass transfer	$k_L a$	$0.6\frac{d_B}{2}$	2.76×10^{-4}	2.76×10^{-4}	s^{-1}	6, 7
Deckwer correlation						
Volumetric coefficient for liquid mass transfer (absorption)	$k_L a$	$0.0086(100\times v_B)^{0.884}$	3.58×10^{-2}	N/A	s^{-1}	12
Volumetric coefficient for liquid mass transfer (desorption)	$k_L a$	$0.0274(100\times v_B)^{0.8}$	9.96×10^{-2}	N/A	s^{-1}	12

Summary of properties and parameter fed into the model

Table S3. Experimentally measured characteristics of photo-anode Ti|Sn^{IV}-Fe_2O_3

Parameter		Symbol	Value	Unit	Technique
Hematite film thickness		x	4.7×10^{-8}	m	Profilometry
Band gap		E_g	2.11	eV	Tauc-plot
Absorptivity		$\alpha_\lambda = f(\lambda)$		m^{-1}	Absorbance UV-Vis region
Relative permittivity		ε_r	38.2	1	Photo current/PEIS analysis[13]
Donor density		n_0	1.92×10^{25}	m^{-3}	Mott-Schottky (Dark)
Charge transfer resistance		$R_t = f(U_{applied})$		$\Omega\ m^{-2}$	PEIS
Surface recombination resistance		$R_r = f(U_{applied})$		$\Omega\ m^{-2}$	PEIS
Flat band	Non-annealed	U_{fb}	0.711 *vs.* RHE	V	Squared photocurrent in 1M NaOH + 0.5M H_2O_2
	400 °C 60 min		0.675 *vs.* RHE	V	
	500 °C 60 min		0.725 *vs.* RHE	V	
Interfacial charge transfer efficiency		$\Phi_{surface} = f(A,B,\phi_{SC})$		1	Fitting of PEIS spectra
Fitting parameter A	Non-annealed	A	2.547×10^{-6}	1	
	400 °C 60 min		1.059×10^{-4}	1	
	500 °C 60 min		1.079×10^{-2}	1	
Fitting parameter B	Non-annealed	B	17.23	V^{-1}	
	400 °C 60 min		15.06	V^{-1}	
	500 °C 60 min		8.255	V^{-1}	
Bulk recombination	Non-annealed	Φ_{bulk}	0.1108	1	Squared photocurrent in 1M NaOH + 0.5M H_2O_2
	400 °C 60 min		0.0888	1	
	500 °C 60 min		0.0702	1	
Exchange current density	Non-annealed	$j_{0,a}$	1.005×10^{-3}	$A\ m^{-2}$	Dark CV at 10 mV s^{-1}
	400 °C 60 min		1.337×10^{-3}	$A\ m^{-2}$	
	500 °C 60 min		8.029×10^{-3}	$A\ m^{-2}$	
Tafel slope	Non-annealed	A_a	0.175	$V\ dec^{-1}$	Dark CV at 10 mV s^{-1}
	400 °C 60 min		0.224	$V\ dec^{-1}$	
	500 °C 60 min		0.454	$V\ dec^{-1}$	

Table S4. Properties of set up and spectrally resolve absorbed photon flux

Parameter		Symbol	Value	Unit	Technique
Temperature		T	298	K	Thermometer
pH		pH	13.6	1	pH-meter
Photon flux		I_0	6.02×10^{21}	$m^{-2}\ s^{-1}$	UV-Vis spectrophotometer
Absorbed photon flux	Non-annealed	$\sum(I_0 - I_x)_\lambda$	2.97×10^{21}	$m^{-2}\ s^{-1}$	Integration of absorbance and photon flux
	400 °C 60 min		2.91×10^{21}	$m^{-2}\ s^{-1}$	
	500 °C 60 min		3.11×10^{21}	$m^{-2}\ s^{-1}$	
Absorbed photon flux times absorption coefficient	Non-annealed	$\sum(I_0 - I_x)_\lambda \alpha_\lambda$	1.71×10^{29}	$m^{-3}\ s^{-1}$	Integration of absorbance and photon flux
	400 °C 60 min		1.70×10^{29}	$m^{-3}\ s^{-1}$	
	500 °C 60 min		1.72×10^{29}	$m^{-3}\ s^{-1}$	
Power intensity		P_0	3646	$W\ m^{-2}$	UV-Vis spectrophotometer
Conductivity of electrolyte (1M NaOH)		$\sigma_{e,a}$ and $\sigma_{e,c}$	20.6	$S\ m^{-1}$	Conductivity Meter
Membrane thickness		l_m	3.30×10^{-4}	m	Taken from supplier

Table S5. Summary of parameter taken from literature or calculated from thermodynamic data

Parameter	Symbol	Value	Unit	Reference
Elementary charge	e	1.6022×10^{-19}	C	
Boltzmann constant	k_B	1.3806×10^{-23}	J K^{-1}	
Vacuum permittivity	ε_0	8.85×10^{-12}	F m^{-1}	
Speed of light	c	3.00×10^{8}	m s^{-1}	
Planck constant	h	6.626×10^{-34}	J s	
Faraday constant	F	96484.6	C mol^{-1}	
Gas constant	R	8.31445	J mol^{-1} K^{-1}	
Reversible potential of O_2 evolution (OER, pH 13.6)	$U_{O_2\|H_2O}$	1.229	V *vs.* RHE	
Reversible potential of H_2 evolution (HER, pH 13.6)	$U_{H_2O\|H_2}$	0	V *vs.* RHE	
Number of electrons transferred for O_2 evolution (OER)	n_{O_2}	4	1	
Number of electrons transferred for H_2 evolution (HER)	n_{H_2}	2	1	
Exchange current density cathode (Pt)	$j_{0,c}$	6.9	A m^{-2}	14
Transfer coefficient for oxidation (Pt)	$\alpha_{ox,c}$	0.5	1	14
Transfer coefficient for reduction (Pt)	$\alpha_{red,c}$	0.5	1	14
Conductivity of substrate (Ti)	σ_a and σ_c	1.8×10^{6}	S m^{-1}	15
Conductivity of membrane (Nafion® 117)	σ_m	10	S m^{-1}	16
Diffusion coefficient of O_2 in membrane (Nafion® 117)	$D_{O_2,m}$	6.2×10^{-11}	m^2 s^{-1}	17
Diffusion coefficient of H_2 in membrane (Nafion® 125)	$D_{H_2,m}$	8.02×10^{-11}	m^2 s^{-1}	18
Saturation concentration of O_2 in membrane (Nafion® 117)	$c_{O_2,sat,m}$	18.7	mol m^{-3}	17
Saturation concentration of H_2 in membrane (Nafion® 125)	$c_{H_2,sat,m}$	7.5	mol m^{-3}	18
Partition coefficient of O_2 membrane | electrolyte	$K_{O_2,m}$	21.01	1	4, 17, 18
Partition coefficient of H_2 membrane | electrolyte	$K_{H_2,m}$	14.42	1	4, 17, 18
Diffusion coefficient of O_2 in electrolyte (1M KOH)	D_{O_2}	1.59×10^{-9}	m^2 s^{-1}	4
Diffusion coefficient of H_2 in electrolyte (1M KOH)	D_{H_2}	3.0×10^{-9}	m^2 s^{-1}	4
Saturation concentration of O_2 in electrolyte (1M KOH)	$c_{O_2,sat}$	0.89	mol m^{-3}	4
Saturation concentration of H_2 in electrolyte (1M KOH)	$c_{H_2,sat}$	0.52	mol m^{-3}	4
Volumetric mass transfer coefficient of O_2 (water)	$k_L a_{O_2}$	1.94×10^{-4}	s^{-1}	5, 8, 10
Volumetric mass transfer coefficient of H_2 (water)	$k_L a_{H_2}$	3.02×10^{-4}	s^{-1}	5, 8, 10
Diffusion coefficient of OH^- in electrolyte (0.26M NaOH)	D_{OH^-}	4.56×10^{-9}	m^2 s^{-1}	19
Proportionality factor of power law of O_2 bubble evolution (1M KOH)	a_{G,O_2}	0.6	1	4
Exponent of power law of O_2 bubble evolution (1M KOH)	n_{G,O_2}	0.39	1	4
Proportionality factor of power law of H_2 bubble evolution (1M KOH)	a_{G,H_2}	1.1	1	4
Exponent of power law of H_2 bubble evolution (1M KOH)	n_{G,H_2}	0.39	1	4

Donor density and flat band potential determination using Mott-Schottky

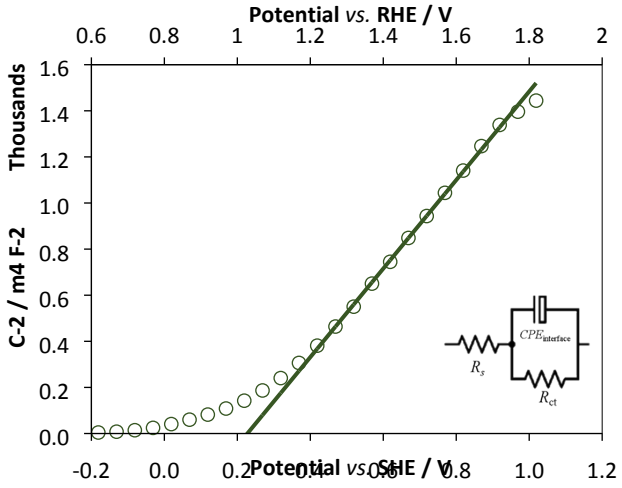

Figure S3. Mott-Schottky plots on Ti|Sn^{IV}-doped α-Fe_2O_3 in 1M NaOH after annealing at 500 ° temperatures. Inset shows the equivalent electrical circuit used to fit the impedance spectra.

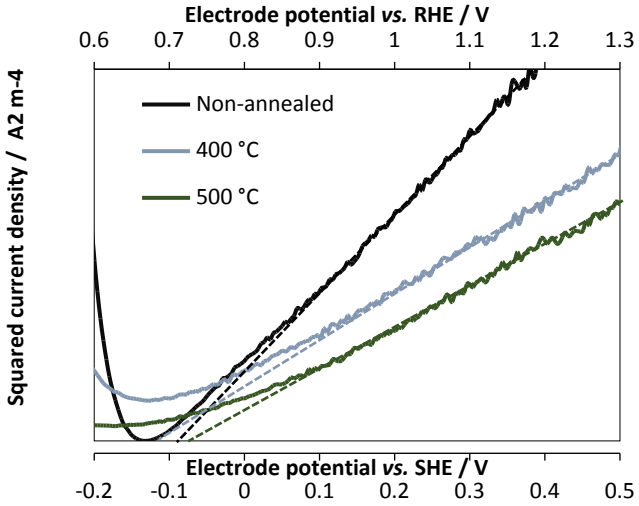

Figure S4. Squared photocurrent (evaluated by subtracting the dark current from the current measured under illumination) of Ti|Sn^{IV}-doped α-Fe_2O_3 after different temperature of annealing in presence of 0.5M H_2O_2 and 3000 W m^{-2} Xe arc lamp.

Table S6. Effects of annealing temperature and time on flat band potential vs. RHE (V) for Ti|Sn^{IV}-doped α-Fe_2O_3 | 1 M NaOH estimated by different methods.

Sample	OCPD (photo) / V 1 M NaOH	OCPD (photo) / V 1 M NaOH + 0.5 M H_2O_2	j_{ph}^2 / A^2 m^{-4}
Un-annealed	0.71	0.68	0.71
400°C 60min	0.67	0.65	0.66
500°C 60min	0.73	0.67	0.72

Absorbed photon flux determination

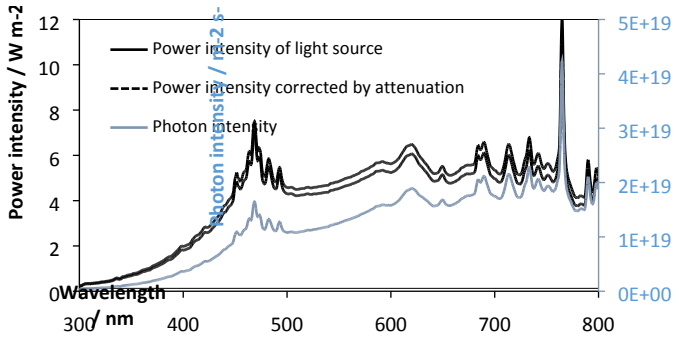

Figure S5. Power intensity before and after correction by electrolyte and quartz window attenuation of the 3600 W m^{-2} Xe arc lamp. Photon flux in the right axis.

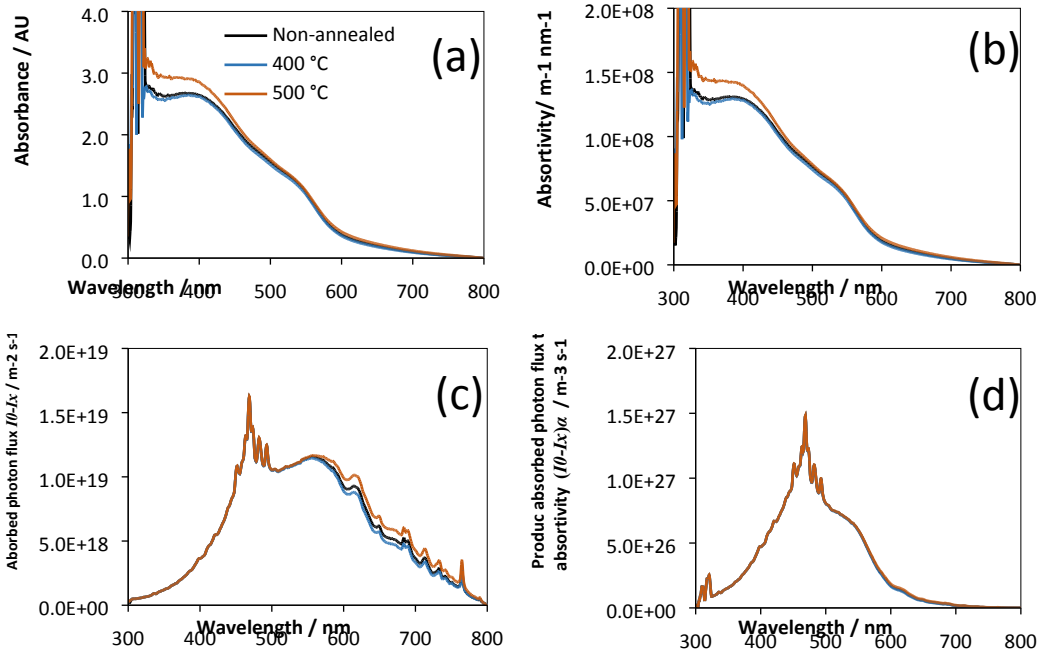

Figure S6. Optical properties of FTO|Sn^{IV}-doped α-Fe_2O_3 non-annealed, 400 °C and 500 °C annealing corrected by attenuation by electrolyte and quartz window. (a) absorbance spectra, (b) absorptivity, (c) absorbed photon flux and (d) product of photon flux and absorptivity.

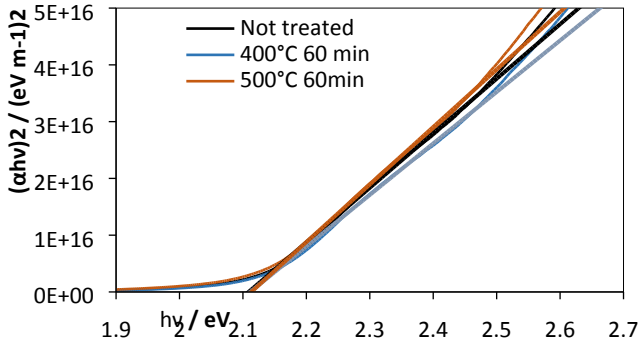

Figure S7. Tauc plot for direct band gap of Sn^{IV}-doped α-Fe_2O_3 on FTO: non-annealed, 400 °C and 500 °C annealing. Hematite film thickness was 47nm.

Estimation of electron-hole recombination in bulk from photo-current in presence and absence of hole scavenger

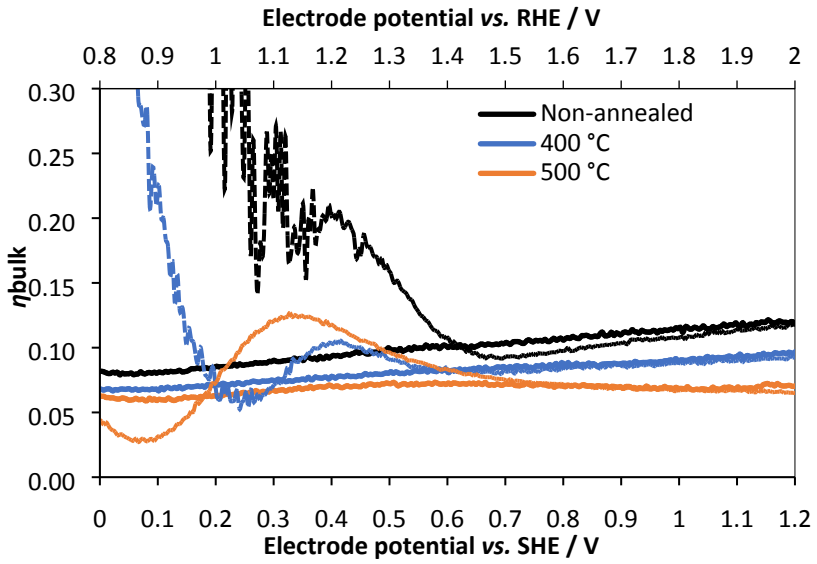

Figure S8. Bulk efficiency estimation using photoresponse and eqn (10) in presence (continuous lines) and absence (dashed lines) of a hole-scavenger. The deviation at low potentials is due to very low currents densities measured in absence of hole scavenger. Photocurrent densities in 1 M NaOH were corrected only for surface recombination rates: dividing the photocurrent density by $\Phi_{surface}$ as a function of potential.

Table S7. Comparison of electron-hole recombination efficiencies in bulk photo-anode calculated from photo-response in presence and absence of hole scavenger as an average between 1.4 and 2.0 V *vs.* RHE.

Sample	Φ_{bulk}	
	1M NaOH + 0.5M H_2O_2	1M NaOH
Ti|Sn^{IV}-doped α-Fe_2O_3 non-annealed	0.1107	0.1044
Ti|Sn^{IV}-doped α-Fe_2O_3 400 °C	0.0888	0.0862
Ti|Sn^{IV}-doped α-Fe_2O_3 500 °C	0.0702	0.0703

Efficiency of gas evolution (f_G) and gas desorption rate with the current density at the cathode and anode.

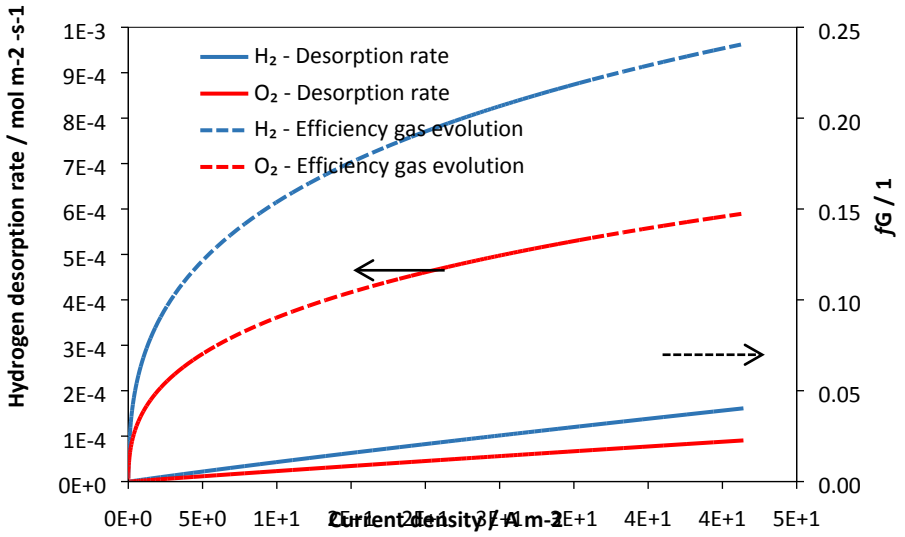

Figure S9. Dependence of efficiency of gas evolution f_G and gas desorption rate on current density at the cathode and photo-anode for hydrogen and oxygen evolution, respectively.

.

Properties of a hypothetical enhanced photo-anode

Table S8. Characterisation of hypothetical photo-anode

Parameter	Symbol	Value	Unit
Film thickness	x	4.7×10^{-8}	m
Band gap	E_g	1.7	eV
		729	nm
Absorptivity	α	1.47×10^{8}	m^{-1}
Relative permittivity	ε_r	40	1
Donor density	n_0	1×10^{25}	m^{-3}
Flat band	U_{fb}	0.1 *vs.* RHE	V
Interfacial charge transfer efficiency	$\Phi_{surface} = f(A,B,\phi_{SC})$		1
Fitting parameter A	A	1.059×10^{-4}	1
Fitting parameter B	B	15.06	V^{-1}
Bulk recombination	Φ_{bulk}	0.5	1
Exchange current	$j_{0,a}$	1.005×10^{-3}	A m^{-2}
Tafel slope	A_a	0.175	V dec^{-1}

Table S9. Properties of set up and absorbed photon flux for an enhanced photo-electrode

Parameter	Symbol	Value	Unit	Comments
Temperature	T	298	K	
pH	pH	13.6	1	
Photon flux	I_0	4.00×10^{21}	m^{-2} s^{-1}	Solar 1.5AM Direct
Absorbed photon flux	$\sum(I_0 - I_x)_\lambda$	1.21×10^{21}	m^{-2} s^{-1}	
Absorbed photon flux times absorption coefficient	$\sum(I_0 - I_x)_\lambda \alpha_\lambda$	1.78×10^{29}	m^{-3} s^{-1}	
Power intensity	P_0	900	W m^{-2}	Solar 1.5AM Direct
Conductivity of electrolyte (1 M NaOH)	σ_a and σ_c	20.6	S m^{-1}	

Fraction of hydrogen originated from desorption and gas evolution at the surface of the cathode.

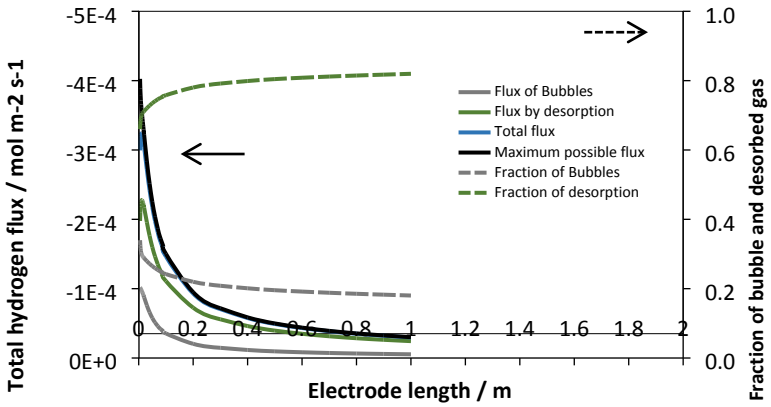

Figure S10. Hydrogen flux due to bubbles at the electrode and desorption under supersaturated conditions (left axis), values are negative as they leave the control volume (electrolyte). Fraction of bubble and desorption rates in the catholyte (right axis) for an enhanced electrode operating at an applied electrode potential of 1 V *vs.* RHE.

Different definitions of efficiency were plotted in Figure S11. STH and ASTH follow the same trend as hydrogen yield. The difference between them is related to the electrical bias, which is accounted in the definition of ASTH efficiency.

$$STH = \left[\frac{E_{H_2} N_{H_2}}{P^o}\right]_{AM\ 1.5G}$$

$$ASTH = \frac{E_{H_2} N_{H_2}}{\left(P^o + j_{ph}\Delta U_{bias}\right)}$$

ABPE and AB-STH are more widely used definitions to compare systems under applied electrical bias in terms of the obtained current and not the hydrogen yield. The only difference between the two is that AB-STH accounts for faradaic efficiency effects, which, in the present case of study, is better replaced by cross-over efficiency. Cross-over efficiency, as defined in the main manuscript, accounts for combined faradaic and cross-over losses. It can be seen how there is a compromise between the cross-over efficiency and the total current density obtained from the system, resulting in a maximum at 0.02 m. This length is longer than the maximum obtained with ASTH, ca. 0.01 m, and it is related to the way ASTH accounts for electrical bias (denominator) compared to AB-STH (numerator). It is worth noticing that the total electrical bias applied to the system decreases with the length electrode, from 1.11 to 1.005 V.

$$ABPE = \left[\frac{j_{ph}\left(E^0 - \left|\Delta U_{bias}\right|\right)}{P^o}\right]_{AM\ 1.5}$$

$$AB - STH = \frac{j_{ph} \times \varepsilon_{H_2} \times (E^0 - \Delta U_{bias})}{P^o}$$

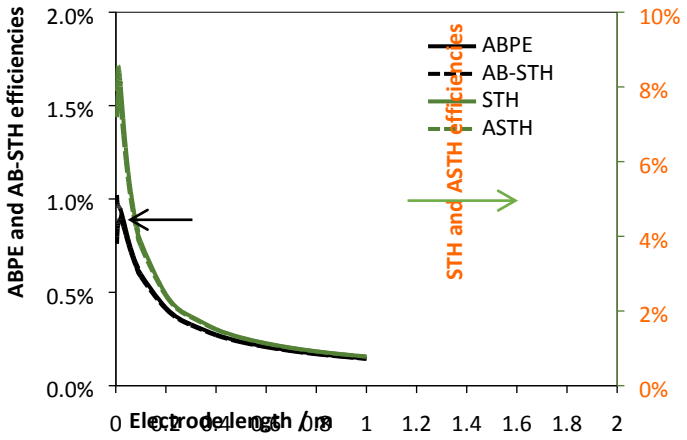

Figure S11. Comparison of the effect of electrode length on different solar-to-hydrogen efficiencies estimated for the enhanced photo-anode operating at 1 V *vs*. RHE.

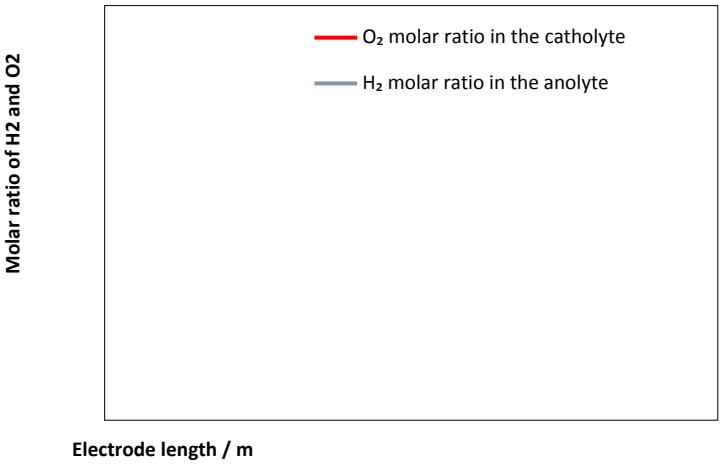

Figure S12. Effect of electrode length on molar fractions of H_2 and O_2 collected in the anolyte and catholyte compartments, respectively; values estimated for the enhanced photo-anode operating at 1 V *vs*. RHE.

Convergence and mesh study

The modelling was performed in COMSOL Multiphysics 5.2a with a Batteries and Fuel Cells module using an Intel® Core™ i7-6700 CPU @ 3.40 GHz processor with 40.0 GB RAM and a 64-bit operating system.

Convergence study

1-D model, anode potential: 1.6 V vs. RHE

Tolerance	Solution time / s	Dark current / A m^{-2}	Photocurrent / A m^{-2}	Hydrogen flux / mol m^{-2} s^{-1}
0.1	1	0.131	20.769	1.0791×10^{-4}
0.01	1	0.131	20.769	1.0791×10^{-4}
0.001	**1**	**0.131**	**20.769**	**1.0789×10^{-4}**
0.0001	1	0.131	20.769	1.0789×10^{-4}

2-D model, anode potential = 1.6 V vs. RHE, electrode length = 0.1 m

Tolerance	Solution time / s	Dark current / A m^{-2}	Photocurrent / A m^{-2}	Hydrogen flux / mol m^{-2} s^{-1}
0.1	60	1.0585	65.048	3.3968×10^{-4}
0.01	62	1.0002	65.667	3.3241×10^{-4}
0.001	**62**	**1.0002**	**65.667**	**3.3241×10^{-4}**
0.0001	63	0.99839	65.676	3.3229×10^{-4}
0.00001	63	0.99839	65.676	3.3229×10^{-4}

Mesh study

1-D model, anode potential: 1.6 V vs. RHE

Domain elements	Solution time / s	Dark current / A m^{-2}	Photocurrent / A m^{-2}	Hydrogen flux / mol m^{-2} s^{-1}
23	0.1	0.131	20.769	1.0789×10^{-4}
102	**1**	**0.131**	**20.769**	**1.0789×10^{-4}**
1001	1	0.131	20.769	1.0789×10^{-4}

2-D model, anode potential = 1.6 V vs. RHE, electrode length = 0.1 m

Domain elements	Solution time / s	Dark current / A m^{-2}	Photocurrent / A m^{-2}	Hydrogen flux / mol m^{-2} s^{-1}
7882	8	1.1684	66.043	3.3273×10^{-4}
26799	18	1.0517	65.771	3.3225×10^{-4}
69530	**62**	**1.0002**	**65.667**	**3.3241×10^{-4}**
115305	87	0.97021	65.607	3.3224×10^{-4}
153344	119	0.96718	65.592	3.3220×10^{-4}
210500	193	0.95232	65.580	3.3241×10^{-4}

Derivation of modified Gartner-Butler equation

The derivation of the modified Gartner-Butler equation was explained in more detailed previously.[13] The nomenclature and symbols of the original references were also updated in here.

According to Butler,[20] the generated electron-hole pairs are a function of incident photons and absorptivity coefficient of the material:

$$G(x) = I_0 \alpha \exp(-\alpha x)$$

Where x is the depth from the surface | electrolyte interface.

The total photocurrent generated due to the absorption of photons in the semiconductor was derived by Gärtner [21]:

$$j_{ph} = eI_o\left[1 - \frac{\exp(-\alpha d_{sc})}{(1+\alpha L_p)}\right] + \frac{ep_0 D_p}{L_p}$$

The first term on the right is associated with the photocurrent due to electron-hole pairs generated in the depletion layer width, d_{sc}. The second term involves the photocurrent generated by diffusion of holes into the bulk of the semiconductor. In this case, the absorptivity coefficient is a function of wavelength, λ, so the photocurrent densities generated will also be a function of λ and the total photocurrent density can be obtained by integration over the wavelength range of the light source.

Later, Butler assumed that for semiconductors with a wide bandgap, e.g. TiO_2 and WO_3, the contribution of the second term due to diffusion can be disregarded. This assumption can also be extended to hematite. Also, if the diffusion length, L_p, is small compared to the absorption depth, α^{-1}, i.e. $\alpha L_p \ll 1,$ then expected photocurrent densities can be simplified to:

$$j_{ph} = eI_o\left[1 - \exp(-\alpha d_{sc})\right]$$

This equation is similar to that proposed initially, $G(x) = I_0 \alpha \exp(-\alpha x)$, and can be obtained after integration of the generation rate of electron-hole pairs from the electrode | electrolyte interface, $x = 0$, to the depletion layer depth, $x = d_{sc}$.

$$j_{ph} = e\int_0^{d_{SC}} G(x)dx$$

$$j_{ph} = -eI_o\left[\exp(-\alpha d_{sc}) - 1\right]$$

The thickness of depletion region is given by:[22]

$$d_{SC} = 2L_{D,eff}\left[\frac{e\Delta\phi_{SC}}{k_B T} - 1\right]^{0.5}$$

Where $L_{D,eff}$ is the effective diffusion length:

$$L_{D,eff} = \left(\frac{\varepsilon_0 \varepsilon_r k_B T}{2 n_0 e^2}\right)^{0.5}$$

Replacing d_{SC} and $L_{D,eff}$, and expanding the exponential term under the assumption that the value inside is much less than one, i.e. $\alpha d_{sc} \ll 1$, then the following equation is obtained:

$$j_{ph(GB)} = \left(\frac{2eI_0^2 \alpha^2 \varepsilon_0 \varepsilon_r}{n_0}\right)^{\frac{1}{2}} (\Delta\phi_{SC})^{\frac{1}{2}}$$

Also, assuming that the band bending in the semiconductor can be expressed as the difference between the applied potential and the flat band, and expressing the photon flux and absorptivity as functions of wavelength:

$$j_{ph(GB)} = \left(\frac{2e\left(\sum_\lambda I_{0,\lambda} \alpha_\lambda\right)^2 \varepsilon_0 \varepsilon_r}{n_0}\right)^{\frac{1}{2}} (U_{applied} - U_{FB})^{\frac{1}{2}}$$

The photocurrent predicted by the modified Gärtner–Butler equation does not account for electron-hole recombination losses in the bulk of the semiconductor and in the electrode | electrolyte interface.

References

1. H. Vogt, *Electrochimica Acta*, 1984, **29**, 167-173.
2. S. Shibata, *Bulletin of The Chemical Society of Japan*, 1963, **36**, 53-57.
3. S. Shibata, *Electrochimica Acta*, 1978, **23**, 619-623.
4. J. M. Chin Kwie Joe, L. J. J. Janssen, S. J. D. van Strelen, J. H. G. Verbunt and W. M. Sluyter, *Electrochimica Acta*, 1988, **33**, 769-779.
5. G. Marrucci and L. Nicodemo, *Chemical Engineering Science*, 1967, **22**, 1257-1265.
6. D. F. McGinnis and J. C. Little, *Water Research*, 2002, **36**, 4627-4635.
7. A. Wüest, N. H. Brooks and D. M. Imboden, *Water Resources Research*, 1992, **28**, 3235-3250.
8. P. Painmanakul, J. Wachirasak, M. Jamnongwong and G. Hebrard, *Engineering Journal*, 2009, **13**, 16.
9. J. B. Joshi and M. M. Sharma, *Transactions of the Institute of Chemical Engineers*, 1979, **57**, 244-251.
10. N. Frossling, *Gerlands Beitrage zur Geophysik*, 1938, **52**, 107-216.
11. W. D. Deckwer, *Bubble Column Reactions*, John Wiley, Chichester, 1992.
12. W. D. Deckwer, R. Burckhart and G. Zoll, *Chemical Engineering Science*, 1974, **29**, 2177-2188.
13. A. Hankin, F. E. Bedoya-Lora, C. K. Ong, J. C. Alexander, F. Petter and G. H. Kelsall, *Energy & Environmental Science*, 2017, **10**, 346-360.
14. W. Sheng, H. A. Gasteiger and Y. Shao-Horn, *Journal of The Electrochemical Society*, 2010, **157**, B1529-B1536.
15. R. W. Powell and R. P. Tye, *Journal of the Less Common Metals*, 1961, **3**, 226-233.
16. Y. Sone, P. Ekdunge and D. Simonsson, *Journal of The Electrochemical Society*, 1996, **143**, 1254-1259.
17. A. T. Haug and R. E. White, *Journal of The Electrochemical Society*, 2000, **147**, 980-983.
18. Z. Ogumi, T. Kuroe and Z. i. Takehara, *Journal of The Electrochemical Society*, 1985, **132**, 2601-2605.
19. S. H. Lee, *Bull. Korean Chem. Soc.*, 2013, **34**, 2925-2930.
20. M. A. Butler, *Journal of Applied Physics*, 1977, **48**, 1914-1920.
21. W. W. Gärtner, *Physical Review*, 1959, **116**, 84-87.
22. R. Memming, in *Comprehensive Treatise of Electrochemistry*, eds. B. E. Conway, J. O. M. Bockris, E. Yeager, S. U. M. Khan and R. E. White, Springer, US, 1983, vol. Volume 7: Kinetics and Mechanisms of Electrode Processes, pp. 529 – 592